



Research paper

SA-49, a novel aloperine derivative, induces MITF-dependent lysosomal degradation of PD-L1



Na Zhang^{a,1}, Yueying Dou^{b,1}, Lu Liu^c, Xin Zhang^a, Xiaojia Liu^a, Qingxuan Zeng^a, Yang Liu^a, Mingxiao Yin^a, Xiujun Liu^a, Hongbin Deng^{a,*}, Danqing Song^{a,*}

^a Institute of Medicinal Biotechnology, Chinese Academy of Medical Sciences & Peking Union Medical College, Beijing 100050, China

^b Pharmacy Department, Hefei BOE Hospital Co., Ltd., Hefei 230011, China

^c Qingdao Women and Children's Hospital, Qingdao University, Qingdao 266034, China

ARTICLE INFO

Article history:

Received 26 November 2018

Received in revised form 25 January 2019

Accepted 25 January 2019

Available online 31 January 2019

Keywords:

Aloperine

PD-L1

Lysosome

MITF

Checkpoint inhibitors

ABSTRACT

Background: Programmed death-ligand 1 (PD-L1) is a T-cell inhibitory checkpoint molecule that suppresses antitumor immunity. Anti-PD-L1 antibodies have shown remarkable promise in treating tumors, but the patient response rate is low. Therefore, small-molecule checkpoint inhibitors blocking PD-L1 function are urgently needed. **Methods:** Changes of protein expression and phosphorylation levels were determined by immunoblotting. The level of Membrane PD-L1 was examined by flow cytometer. Cytotoxicity of T cells and NK cells toward tumor cells were detected using LDH and cell index assays. Lysosome function was investigated by NAG assay. Changes in lysosomal-related genes were measured by RT-PCR. In vivo anti-NSCLC cancer effects were assessed using C57BL/6 mice bearing Lewis tumor xenografts.

Findings: We identified SA-49 as a new regulator of PD-L1 expression from a series of novel aloperine derivatives. SA-49 decreased the expression of PD-L1 in NSCLC cells and enhanced the cytotoxicity of co-cultured T and NK cells toward tumor cells. Importantly, lysosomal pathway contributed to SA-49-mediated down-regulation of PD-L1. SA-49 increased the biogenesis of lysosome and promoted translocation of PD-L1 to lysosome for proteolysis, which was associated with nuclear translocation of MITF. SA-49-induced MITF translocation acted through activation of PKC α and subsequently suppression of GSK3 β activity. Furthermore, SA-49 suppressed Lewis tumor xenograft growth by activating immune microenvironment in C57BL/6 mice.

Interpretation: Our data demonstrate that SA-49 can be used to regulate PD-L1 in cancer cells and trigger its degradation by activating lysosome function.

© 2019 Published by Elsevier B.V. This is an open access article under the CC BY-NC-ND license (<http://creativecommons.org/licenses/by-nc-nd/4.0/>).

1. Introduction

Improved understanding of the immune regulation in cancer development has led to impressive advances in the field of cancer immunotherapy over the last decade. Cancer cells often escape immune surveillance by manipulating the expression of immune checkpoint molecules on cancer or matrix cells [1]. Programmed death-ligand 1 (PD-L1, also known as B7-H1 or CD274) is a type I integral membrane glycoprotein that expressed at the surface of tumor cells [2,3]. PD-L1 acts as a T-cell inhibitory checkpoint molecule which can inactivate tumor-infiltrating immune cells that express cell surface programmed death-1 (PD-1, also known as CD279) [4,5]. When PD-1 was bound by PD-L1, the naive CD4⁺ T cells differentiate into regulatory T (Treg)

cells, and play the role of Treg-suppressive functions, thus inhibiting the immune activation and effector response [6]. Beside of immune-inhibitory effect, PD-L1 can also act as an oncogene by sending limiting tumor cell apoptosis signals [7]. PD-L1 expression in non-small cell lung cancers (NSCLC) is a hallmark of adaptive resistance and its expression is often used to predict the outcome of PD-1 and PD-L1 immunotherapy treatments [8]. Thus, blocking the PD-1/PD-L1 axis is recognized as the attractive target for cancer immunotherapy, including NSCLC [9,10]. However, clinical benefits do not occur in all patients and new approaches are needed to improve the PD-1 or PD-L1 immunotherapies.

The antibody-based PD-1/PD-L1 inhibitors, such as nivolumab, avelumab and atezolizumab, have achieved durable treatment effects in patients with various cancer types including NSCLC [11–13]. While these antibody-based therapies show impressive clinical activity, they suffer from several shortcomings, including poor tissue and tumor penetration, stability, the lack of oral bioavailability, immunogenicity, and difficult and costly production [14]. In addition, currently antibody drugs recognize only a small fraction of extracellular proteins that are

* Corresponding authors.

E-mail addresses: hdeng@imb.pumc.edu.cn (H. Deng),

songdanqing@imb.pumc.edu.cn (D. Song).

¹ These authors contributed equally to this work.

Research in context

Evidence before this study

The antibody-based PD-1/PD-L1 inhibitors, such as nivolumab, avelumab and atezolizumab, have recognized as the attractive target for cancer immunotherapy. However, clinical benefits do not occur in all patients and new approaches are needed to improve the PD-1 or PD-L1 immunotherapies.

Added value of this study

Findings from this study indicate that SA-49 decreased the expression of PD-L1 in NSCLC cells and activated immune microenvironment in C57BL/6 mice bearing Lewis tumor xenograft by activating MITF-dependent lysosome function.

Implications of all the available evidence

SA-49 may be an effective small molecule immune checkpoint inhibitor that blocks PD-1 and PD-L1 axis and provides additional methods for cancer treatment.

regarded as cancer biomarkers [15]. Compared to antibody drugs, small molecule immune checkpoint inhibitors could offer inherent advantages in terms of favorable pharmacokinetics and druggability, such as better oral bioavailability, higher tissue and tumor penetration, reasonable half-lives etc. [16,17], thereby providing additional methods for cancer treatment and achieving better therapeutic effects.

Aloperine is a kind of quinolizidine alkaloid extracted from the leaves of *Sophora alopecuroides* L., possesses anti-inflammatory, anti-allergenic, and anti-viral effects [18,19]. Recently, aloperine was also shown antitumor effects on multiple malignant neoplasms including prostate cancer, myeloma, and lung carcinoma [18,20]. These observations prompted us to hypothesize that aloperine or its analogues may be a good candidate drug for the prevention and treatment of tumor. To address this feasibility, a library of aloperine analogues was constructed in our lab [21], and the antitumor effect of these analogues via inhibiting PD-L1 function was conducted. Interestingly, we found that SA-49, a novel sulfonyl-substituted aloperine derivative, decreased the protein level of PD-L1 in NSCLC cells and mice bearing Lewis tumor xenografts. We showed that SA-49 induces nuclear translocation of melanogenesis associated transcription factor (MITF) by activating protein kinase C α (PKC α) and subsequently suppressing glycogen synthase kinase 3 β (GSK3 β), therefore triggers lysosome-based degradation of PD-L1.

2. Materials and methods

2.1. Antibodies and reagents

SA-49 was synthesized as described previously and dissolved in DMSO [21]. LY294002, Go6976, 5Z-7-Oxozeaenol and Torin1 were purchased from Selleck (Beijing, China). Cycloheximide (CHX), MG132, and Bafilomycin (Baf) were purchased from Sigma (St. Louis, MO, USA). Antibodies against PD-L1, TFEB, MITF, H3, PKC α , p-GSK3 β (Ser9), cleaved caspase 9 and 3 were purchased from Cell Signaling (Danvers, MA, USA). Anti-GSK3 β and GAPDH antibodies were purchased from Santa Cruz (Santa Cruz, CA, USA). Anti-PD-L1-PE, IgG-PE and FoxP3 antibodies were purchased from eBioscience (San Diego, CA, USA). Antibodies against p-PKC α (T638), CD3 and Ki67 were obtained from Abcam (Cambridge, MA, USA). The probes LysoTracker and DAPI were purchased from Invitrogen (Carlsbad, CA, USA). Human PD-1 Fc

recombinant protein and IL-2 were purchased from R&D Systems (Minneapolis, MN, USA).

2.2. Plasmids

The plasmid GFP tagged-PD-L1 (GFP-PD-L1) was constructed by inserting the coding sequence of human PD-L1 into the vector of pCDNA3-GFP at *EcoRI* and *XhoI* sites. The pEGFP-MITF (#38131) and pEGFP-TFEB (#38119) plasmids were purchased from Addgene (Cambridge, MA, USA).

2.3. Cell culture

NSCLC cell lines A549, NCI-H157, NCI-H1975, NCI-H1299, NCI-H460 and Lewis cells were purchased from Shanghai Institutes for Biological Sciences (Shanghai, China). Activated T and NK cells were purchased from Stemcell Technologies (Vancouver, BC, Canada). A549 cells were cultured in DMEM/F-12 medium, and all the other cells were cultured in RPMI1640 medium (Gibco, NY, USA). The culture medium was supplemented with 10% fetal bovine serum (Hyclone, UT, USA), 100 U/mL penicillin, and 100 μ g/mL streptomycin. Cells were incubated in a humidified atmosphere with 5% CO₂ at 37 °C. No mycoplasma contamination of cell lines was found using DAPI staining. All cells used in this study were within twenty passages after receipt or resuscitation.

2.4. Small interfering RNA knockdown and transfection

TFEB siRNA (5'-UGUAAUGCAUGACAGCCUG-3'), TFEB3 siRNA (5'-AUCCUG CUCUCUUCAGUGTT-3'), MITF siRNA (5'-GGUGAAUCGGAUCAUCAAG-3'), PKC α siRNA (5'-AUUUCAUACAACAGGAGCCTT-3'), PKC β siRNA (5'-UUUA GCAUCUCUUCAGAGGT-3'), Control siRNA (5'-UUCUCCGAACGUGUCACG UTT-3') were purchased from GenePharma (Shanghai, China). For siRNA-mediated silencing, cells were transfected with 100 nM of target siRNA and a control siRNA using Vigofect (Vigorous Biotechnology, China) according to the manufacturer's recommendations. 48 h post-transfection, the protein expression was analyzed by IB.

2.5. T and NK cell-mediated tumor cell-killing assay

Cytotoxicity of human Jurkat T cells against A549 cells was assessed with lactate dehydrogenase (LDH) release assay as previously described [22]. T cells were activated by incubation with anti-CD3 antibody (100 ng/mL) and IL-2 (10 ng/mL). A549 cells were freshly plated at 5×10^3 /well in 96-well plates and pretreated with or without SA-49, SA-14 for 2 h, followed by IFN- γ (10 ng/mL) stimulation for 16 h. A549 cells were washed and then co-cultured with T cells at 1:10 in triplicate in RPMI 1640 plus 10% FBS. Four hours later, cytotoxicity assay was conducted using non-radioactive LDH release assay using a cytotoxicity detection kit (CytoTox 96, Promega, Madison, WI, USA) as the manufacturer's instructions.

NK cell-mediated tumor cell-killing assay was performed by the xCELLigence system (ACEA Biosciences, San Diego, CA, USA) [22]. Briefly, 50 μ L of full medium was placed in each well of the E-plate 16 for 30 min firstly. The final volume was adjusted to 100 μ L by adding additional 50 μ L medium containing of 1×10^3 H460 cells. Each treatment includes two replicates. After treated with the indicated conditions for 24 h, NK cells were added at the ratio of 1:5. Cell index values were measured by continuous impedance recordings every 15 min. The results were analyzed using the real-time cell analysis software supplied by the company.

Cell viability was detected according to CellTiter 96 Aqueous One Solution Cell Proliferation Assay (MTS assay, Promega) as described before [23].

2.6. Immunoblotting

Immunoblotting (IB) was performed as described previously [23]. Briefly, cells were washed twice with ice-cold PBS and lysed in M2 lysis buffer (20 mM Tris-HCl, pH 7.5, 150 mM NaCl, 10 mM β -glycerophosphate, 5 mM EGTA, 1 mM sodium pyrophosphate, 5 mM NaF, 1 mM Na_3VO_4 , 0.5% Triton X-100, and 1 mM DTT) supplemented with protease inhibitor cocktail. Proteins were separated by SDS-PAGE and electrically transferred to a polyvinylidene difluoride membrane. The membrane was probed with the appropriate primary antibody and a HRP-conjugated secondary antibody. Blots were visualized by Tanon 5200 system (Tanon, Shanghai, China).

2.7. PD-L1 and PD-1 interaction assay

To measure the PD-1 and PD-L1 protein interaction in vitro, cells were fixed in 4% paraformaldehyde for 15 min firstly, and followed by incubated with human recombinant PD-1 Fc protein for 1 h at room temperature. Then cells were probed with anti-human Alexa Fluor 488 dye conjugated Fc secondary antibody. Nuclei were stained with DAPI and the green fluorescence was visualized by a microscope (Zeiss, Axio Vert.A1) [2].

2.8. Membrane PD-L1 analysis

Cells treated with SA-49 for the indicated time were collected and incubated with anti-PD-L1-PE antibody for 30 min at 4 °C. The conjugate PE fluorescence was quantitatively analyzed by FACSCalibur flow cytometer and CellQuest software (BD Biosciences, Sparks Glencoe, MD, USA).

2.9. β -N-acetylglucosaminidase (NAG) assay

NAG assays were performed using a kit from Sigma (CS0780) as described before [23]. Briefly, cells treated with SA-49 or Torin 1 for 3 h were lysed in RIPA buffer (250 μ l). Ten micrograms of cell lysates were measured in triplicate for NAG activity following the protocol provided by the supplier.

2.10. LysoTracker Red staining

Lysosomes were labeled by incubating cells with the LysoTracker Red DND-99 dye (50 nM) (Invitrogen, L-7528) at 37 °C for 30 min [24]. The medium was aspirated and washed twice with PBS quickly to remove the unbound dye. Red fluorescence was visualized by a fluorescence microscope (Zeiss, Axio Vert.A1).

2.11. Nuclear and cytosolic fractionation

Nuclear fractions were extracted from cell homogenates by Nuclear/Cytosol Fractionation Kit (Bioss; K2660–25) according to the manufacturer's protocol. Briefly, cells were centrifuged at 600 \times g for 5 min at 4 °C. The pellet added CEB was centrifuged at 16,000 \times g for 5 min at 4 °C, and the resulting supernatant fraction was collected as cytosolic fraction. The pellet fractions were subjected to additional centrifugation. The final supernatant fraction was nuclear section described in the procedure. Samples were subjected to IB.

2.12. Quantitative real-time PCR (qRT-PCR)

Total RNA was isolated from cells using EasyPure RNA Kit (Transgen, Beijing, China) as recommended by the manufacturer. A reverse-transcription kit (Bio-Rad) was used to reverse transcribe RNA (1 μ g) in a 20 μ l reaction mixture. Quantification of gene expression was performed using a real-time PCR system (Bio-Rad iQ5 Real Time PCR) in triplicate. Amplification of the sequence of interest was normalized

with the reference endogenous gene GAPDH. The primer of target genes were as following: *Pd-1* (sense 5'-TCACTTGGAATCTGGGAGC-3'; anti-sense 5'-CTTT GAGTTTGATCTTGGATGCC-3'); *Atp6v1h* (sense 5'-GGAAGTGTACAGATGATC CCA-3', anti-sense 5'-CCGTTTGCCTCGTGA TAAT-3'); *Mitf* (sense 5'- TACAGTC ACTACCAGGTGCAG-3', anti-sense 5'-CCATCAAGCCAAAATTTCTT-3'); *Ctsb* (sense 5'-AGTGGAGAATGGCA CACCTA-3', anti-sense 5'-AAGAAGCCATTGTC ACCCA-3'); *Ctsd* (sense 5'-AACTGCTGGACATCGCTTGCT-3', anti-sense 5'-CAT TCTTCA CGTAGGTGCTGGA-3'); *Lamp1* (sense 5'-ACGTTACAGCGTCCAGCTC AT-3', anti-sense 5'-TCTTTGGAGCTCGCATTGG-3'); *map1lc3b* (sense 5'-CGCACC TTCGAACAAAGAGT-3', anti-sense 5'-AGCTGCTTCTACCCT TGTA-3'); *Atg9b* (sense 5'- ACCTCTCTCTCTTCAT-3', anti-sense 5'-GTGGGAGGGAAAAT GAGGA-3'); *Gapdh* (sense 5'-TGCACCACCAA CTGCTTAGC-3', anti-sense 5'-GG CATGGACTGTGGTCATGAG-3').

2.13. In vivo effect of SA-49

The animal procedures were carried out with the approval of the Animal Ethics Committee of the Institute of Medicinal Biotechnology, Chinese Academy of Medical Sciences. Two-month-old specific pathogen free female C57BL/6 mice weighing 18–22 g were purchased from Beijing Vital River Laboratory Animal Technology (Beijing, China). The mice were inoculated subcutaneously with 5×10^6 Lewis cells. When the average tumor volume reached approximately 50 mm³, mice were divided into four groups randomly ($n = 8$) and treated with 20 mg/kg SA-49, 50 mg/kg SA-49, 100 mg/kg SA-49 and vehicle respectively. The drugs were administered via intragastric injection every day. The vehicle group was administered with 0.5% sodium carboxymethyl cellulose (CMC). Body weight and tumor volume were examined every day after the first administration, and the tumor volumes were calculated using the following equation: Tumor volume (mm³) = $1/2 \times (\text{tumor length}) \times (\text{tumor width})^2$. On the 20th day, the mice were sacrificed, and the blood, major organs (heart, liver, spleen, lung, thymus and kidney) samples were collected. Related biochemistry indicators in serum samples were tested by automated biochemistry analyzer SYNCHRON CX4 PRO (Beckman Coulter, Brea, California, USA). The harvested organs (heart, liver, spleen, and kidney) were fixed in 4% paraformaldehyde, processed into paraffin routinely, stained with haematoxylin and eosin (H&E) and captured by microscope.

2.14. Immunohistochemistry

For immunohistochemistry, tumor tissues were fixed in fresh 10% formaldehyde and cut to four-micrometer thick paraffin sections. After incubated with primary antibodies against PD-L1, FoxP3, CD3, Ki67 and Cleaved Caspase 3 (1:300) for the determination of relative protein expression, PBS was used to replace the primary antibody for the negative control. The slides were probed with a HRP-labeled secondary antibody for 30 min. Subsequently, these slides were counterstained with DAB. Images were obtained using fluorescence microscopy (Zeiss, Axio Vert.A1). For PD-L1, the percentage of positive tumor cell surface staining was scored as 0 (<5%), 1+ (≥ 5 –20%), 2+ (≥ 20 –50%) or 3+ (≥ 50 %). FoxP3, CD3, Ki67 and cleaved caspase 3 stains were quantified by counting the number of positive cells in high magnification.

2.15. Statistics

Results are presented as mean values \pm standard error of independent triplicate experiments. All statistical analyses were performed by using two-tailed Student's *t*-test and *p*-values of <0.05 were considered statistically significant.

3. Results

3.1. Identification of SA-49 as a new regulator of PD-L1 expression

We used H460, one of the human NSCLC cell lines, to start our chemical screen by examining the ability of a series of novel aloperine derivatives (Fig. 1a) to alter PD-L1 expression. PD-L1 was selected as our object because therapies targeting at the PD-1/PD-L1 axis have achieved clinical success. Unexpectedly, we found that SA-49, [12 N-(1-methyl-1H-imidazol-4-yl) sulfonyl aloperine, Supplementary Fig. 1a], could efficiently reduce the constitutive PD-L1 expression in H460 cells (Fig. 1b). Although SA-51 also reduced the constitutive PD-L1 expression, it caused massive cell death within 12 h of drug administration (data not shown), thus it was excluded for the further study. In addition, SA-49 failed to affect H460 cell viability at concentration up to 100 μ M (Supplementary Fig. 1b). SA-49 (10–40 μ M) treatment did not result in obvious activation of cleaved caspase 9 and caspase 3 compared with Tasisulam-treated positive control (Supplementary Fig. 1c) [25]. Furthermore, SA-49 (20 or 40 μ M) treatment did not change the apoptotic rate in H460 cells as compared with Tasisulam-treated control (Supplementary Fig. 1d). Altogether, these data suggest SA-49 reduces PD-L1 expression but shows little cytotoxic effects on NSCLC cells. Therefore, 10–40 μ M SA-49 was used for the subsequent experiments described in this study.

3.2. SA-49 attenuates constitutive and inductive PD-L1 expression in NSCLC cells

We further examined the ability of SA-49 down-regulation of PD-L1 in NSCLC cells. The changes of constitutive PD-L1 expression in H157, H1975 or H460 cells were examined by immunoblotting (IB). SA-49 treatment significantly reduced constitutive PD-L1 expression in NSCLC cells in both time- and concentration-dependent manners (Fig. 1c and d). As tumor cell surface PD-L1 can be upregulated in response to IFN- γ by activated T cells [26], we next examined whether inductive PD-L1 expression could be affected by SA-49. To this end, A549 and H1299 cells were used as basal PD-L1 level was almost undetectable and IFN- γ induced dramatically PD-L1 expression in those cells. Indeed, SA-49 attenuated IFN- γ -induced PD-L1 expression in both A549 and H1299 cells (Fig. 1e). Next, we examined whether SA-49 regulates membranous PD-L1 expression. Flow cytometry assay revealed that SA-49 significantly reduced the cell surface PD-L1 in H157 cells, indicating SA-49 could also reduce the PD-L1 conveyed to the plasma membrane (Fig. 1f and g). Altogether, these results suggest that SA-49 decreased both the constitutive and inductive PD-L1 expression in NSCLC cells.

3.3. SA-49 enhances the cytotoxicity of T and NK cells

When PD-L1 on cancer cells binds to PD-1 on tumor-infiltrating lymphocytes, PD-L1-induced inhibitory signal shuts down their antitumor activity [27]. We next examined whether SA-49-treated cancer cells reduced their ability to bind to PD-1. A cell imaging approach was used to re-create the interaction between PD-L1 and PD-1 in vitro [2]. Cells treated with SA-49 were incubated with recombinant PD-1 Fc protein together with Alexa Fluor 488 dye conjugated Fc antibody. The interaction between PD-L1 and PD-1 on the plasma membrane was reflected by the green fluorescence. Weaken green fluorescence in SA-49-treated H460 cells showed that their ability to bind to PD-1 was significantly reduced, indicating PD-L1 became subdued in NSCLC cells after SA-49 treatment (Fig. 2a and b). To evaluate whether SA-49 or the related aloperine derivative SA-14 could increase T cells activity, we co-cultured A549 cells with activated T cells, the cytotoxicity of co-cultured T cells was detected by LDH releasing assay. IFN- γ neutralized T cell-mediated cell death, whereas SA-49, but not SA-14 treatment significantly reversed the IFN- γ -reduced cytotoxicity of T cells (Fig. 2c).

Meanwhile, cell impedance assay was used to measure the cytotoxicity of NK cells toward co-cultured H460 cells. The reduced cell index of H460 cells after SA-49 instead of SA-14 treatment further confirmed that SA-49 could increase the cytotoxicity of NK cells (Fig. 2d). Taken together, these results suggest that SA-49 enhances the cytotoxicity of T and NK cells toward NSCLC by down-regulation of PD-L1 expression.

3.4. Lysosomal pathway contributes to SA-49-mediated down-regulation of PD-L1

Next, we investigated the mechanisms behind the above described SA-49-induced PD-L1 down-regulation. To this end, we firstly examined whether SA-49 affects PD-L1 expression at the mRNA level. Luciferase reporter assay revealed that IFN- γ -induced PD-L1 promoter activity did not show a significant difference in the presence or absence of SA-49 (Fig. 3a). Simultaneously, real-time PCR results also revealed that there were no changes of PD-L1 mRNA level in IFN- γ -stimulated or unstimulated cells exposed to SA-49 (Fig. 3b and c), indicating that SA-49 provides translational control of PD-L1. To confirm the translational regulation of PD-L1 by SA-49, NSCLC cells were exposed to the protein translation inhibitor cycloheximide (CHX). In the presence of CHX, the turnover rate of PD-L1 in SA-49-treated cells was faster than that in untreated or SA-14-treated cells (Fig. 3d and e; Supplementary Fig. 2a), suggesting SA-49-triggered PD-L1 down-regulation is predominantly controlled at the protein level.

At least two systems exist for protein degradation, including the ubiquitin- proteasome and lysosomal pathways [28]. Indeed, when H460 cells were treated with proteasome inhibitor MG132 or lysosomal inhibitor Bafilomycin (Baf), we found that the degradation of PD-L1 was restored by MG132 or Baf (Fig. 3f), which is consistent with previous reports that PD-L1 exerts both the proteasome- [29,30] and lysosome-dependent [31] degradation pathways. However, when H460 cells co-treated with SA-49 and MG132 or Baf, PD-L1 degradation was completely restored by Baf but not MG132 (Fig. 3g). Moreover, SA-49 did not catalyze ubiquitination of PD-L1 (Supplementary Fig. 2b). Therefore, it is plausible to speculate that the lysosome function was regulated by SA-49, resulted in the accelerated degradation of PD-L1. Taken together, these results suggest that SA-49-mediated PD-L1 degradation is mediated through lysosome-dependent pathway.

3.5. SA-49 increases the biogenesis of lysosome and promotes translocation of PD-L1 to lysosome

To confirm lysosomal function was indeed affected by SA-49, we examined the change of lysosome activity using LysoTracker Red. Interestingly, SA-49 induced an obvious increase in LysoTracker Red staining, similar to that caused by Torin1 (Fig. 4a and b). To further confirm our findings, we investigated the changes of lysosomal-associated genes in the presence of SA-49. In agreement with the LysoTracker Red staining results, we observed that SA-49 upregulated many lysosome-related genes including *mitf*, *lamp1*, *vps11* etc. (Fig. 4c). Meanwhile, SA-49 increased lysosomal protease activities in H460 cells, as measured by β -N-acetylglucosaminidase (NAG) assays (Fig. 4d).

It has been reported that PD-L1 contains a signal peptide including a tyrosine based motif YWHL, which enables the intracellular PD-L1 locating in the lysosomal compartment [32]. We thus hypothesized that SA-49 promotes translocation of PD-L1 to lysosome. Fluorescent microscopy analysis indicated that an increased amount of GFP-PD-L1 was found to localize with LysoTracker Red in H460 cells (Fig. 4e and f), indicating that SA-49 promoted PD-L1 translocation to lysosome. Taken together, these data suggest that SA-49 induces biogenesis of functional lysosomes, thereby promoting the translocation of PD-L1 to lysosomes for proteolysis.

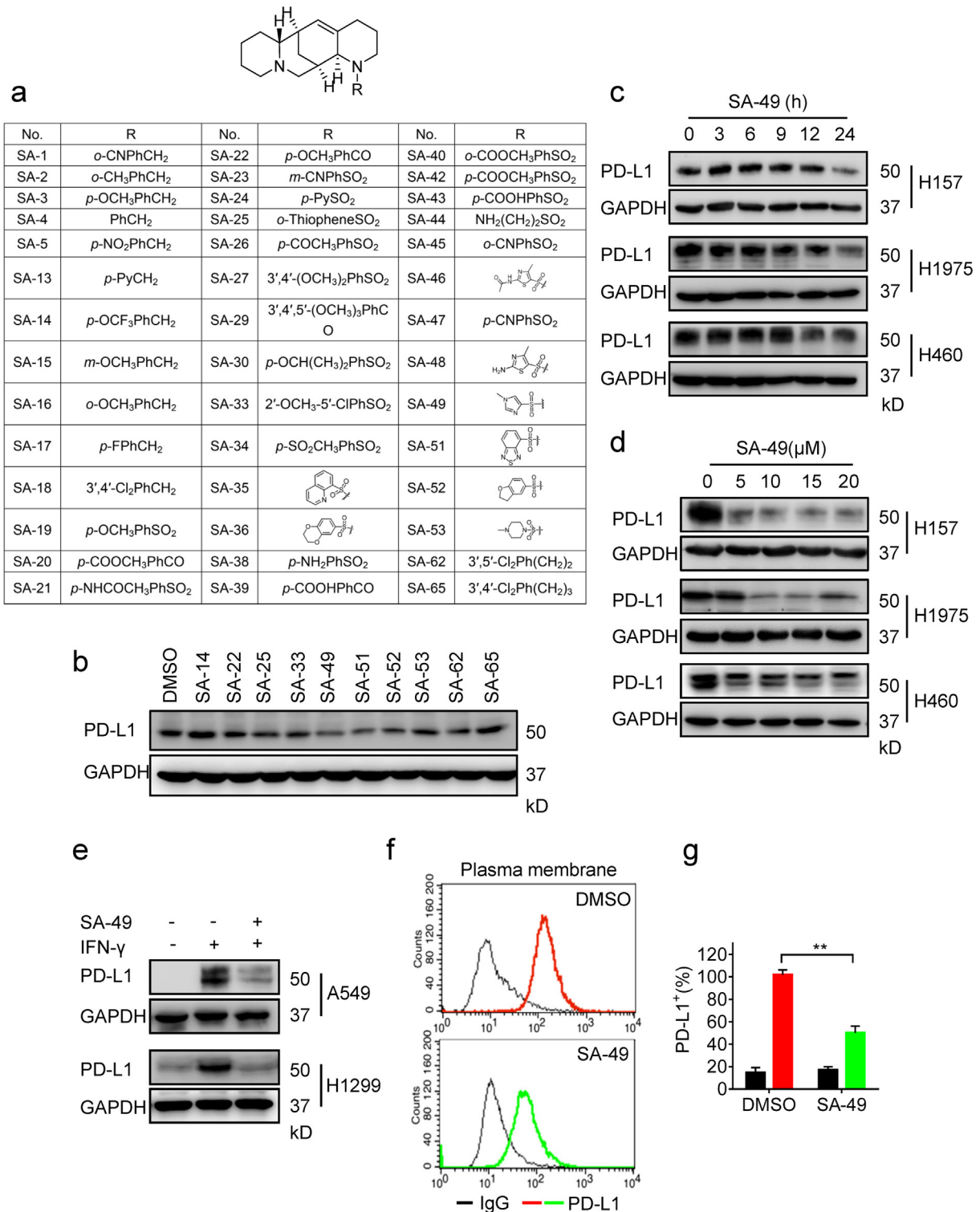


Fig. 1. Identification of SA-49 as a PD-L1 regulator. (a) Chemical structures of aloperine derivatives. (b) IB analysis of PD-L1 expression in H460 cells treatment with the indicated aloperine derivatives (10 μM) for 24 h. (c and d) H157, H1975 and H460 cells were treated with 10 μM SA-49 for the indicated times (c), or treated with different concentrations of SA-49 for 24 h (d), PD-L1 expression levels were detected by IB. (e) A549 or H1299 cells were pre-treated with 10 μM SA-49 for 2 h, then stimulated with 5 ng/mL IFN-γ for 24 h, PD-L1 expression levels were detected by IB. (f) H157 cells were treated with SA-49 for 24 h, the plasma membrane PD-L1 was detected by flow cytometry. The dark curve represented the expression of isotype control, red or green curve represented the expression of PD-L1. (g) Statistic of PD-L1 intensity in (f). ***p* < 0.01 compared with DMSO group (*n* = 3, Student's *t*-test).

3.6. SA-49 triggers MITF-dependent PD-L1 degradation

Lysosome biogenesis can be triggered by the Mit/TFE family, including TFEB, TFE3 and MITF, which increasing the number of lysosomes and promoting protein degradation [33]. On the basis of the observation that

SA-49 triggers biogenesis of lysosomes, we next sought to determine the role of TFEB, TFE3 and MITF in SA-49-induced PD-L1 degradation. To this end, we knocked down TFEB, TFE3 and MITF expression by siRNA in H460 cells (Supplementary Fig. 3). Compared to control cells, silencing of MITF, but not TFEB or TFE3, significantly inhibited SA-49-

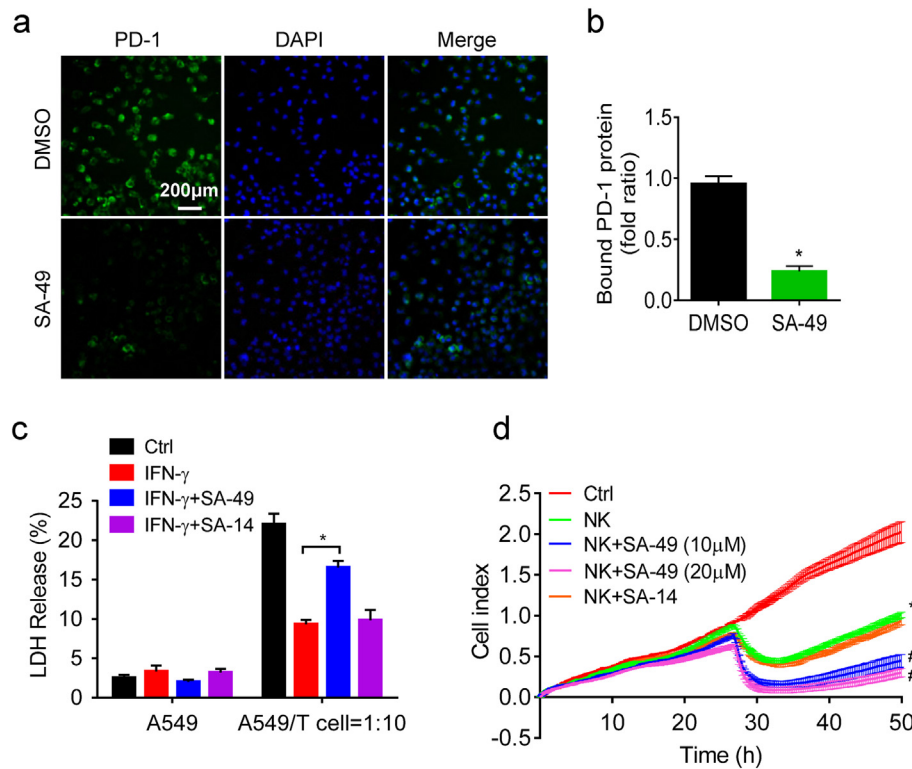


Fig. 2. SA-49 enhances the cytotoxicity of T and NK cells. (a) PD-L1/PD-1 binding assay in H157 cells treated with SA-49 (10 μ M, 24 h). The nuclei were stained with DAPI. (Scale bar, 200 μ m). (b) Bound PD-1 was calculated according to the intensity of green fluorescence. * $p < 0.05$ compared with DMSO group ($n = 3$, Student's t -test). (c) LDH releasing assay measuring T cell-mediated tumor cell killing in A549 cells pre-treated with SA-49 (10 μ M, 2 h) or SA-14 (20 μ M, 2 h), followed by IFN- γ (5 ng/mL, 24 h) stimulation. (d) Cell impedance assay analyzing NK cell-mediated tumor cell killing in H460 cells treated with SA-49 (10 μ M or 20 μ M), SA-14 (20 μ M) for 24 h. * $p < 0.05$ compared with control group (Student's t -test); # $p < 0.05$ compared with NK cells treated group (Student's t -test).

induced PD-L1 degradation (Fig. 5a). Accordingly, SA-49 induced efficient nuclear translocation of EGFP-MITF, but not EGFP-TFEB, when A549 cells transfected with EGFP-TFEB or EGFP-MITF (Fig. 5b and c). In addition, IB analysis of endogenous MITF in nuclear and cytosolic fractionations revealed that SA-49 treatment induced an increase of MITF in the nuclear fraction (Fig. 5d). MITF can directly bind to CLEAR element in the promoters of lysosomal genes [34]. Subsequently, we found that SA-49 increased the CLEAR luciferase activity in a concentration-dependent manner (Fig. 5e).

We used MITF siRNA to further investigate the relevance of MITF on SA-49-induced lysosome biogenesis and PD-L1 degradation. LysoTracker Red staining assay indicated that silencing of MITF significantly inhibited SA-49-induced lysosome increase (Fig. 5f and g). Furthermore, SA-49-increased lysosome NAG activity was also abolished by MITF knockdown (Fig. 5h). Collectively, these data suggest that SA-49 induces MITF nuclear translocation and subsequences PD-L1 degradation in NSCLC cells.

3.7. PKC α -GSK3 β signaling is required for SA-49 action

We next aimed to clarify the molecular basis behind the above described SA-49-induced MITF nuclear translocation. Recently, mammalian target of rapamycin complex 1 (MTORC1) has emerged as a repressor of lysosomal transcriptional biology via directly phosphorylating MiT/TFE proteins on multiple conserved residues [35]. Yet, SA-49 did not alter MTORC1 signaling, as measured by phosphorylation of its substrates RPS6/S6 (ribosomal protein S6) and EIF4EBP1/4E-BP1 (eukaryotic translation initiation factor 4E binding protein 1) (Supplementary Fig. 4), suggesting that SA-49 affects MITF localization via an MTORC1-independent mode of action. On the other hand, GSK3 β inhibition has been reported to regulate MITF phosphorylation thus triggers its nuclear translocation [34,36], we therefore examined the potential

roles of GSK3 β in modulating SA-49-mediated MITF nuclear translocation. To this end, we examined whether SA-49 could regulate GSK3 β activity in NSCLC cells. IB analysis confirmed that treatment with SA-49 in H460 cells resulted in a significant increase of phosphorylated GSK3 β at Ser 9 (Fig. 6a, upper panel), which indicating SA-49 inhibits GSK3 β activation. In addition, the phosphorylation of glycogen synthase (p-GS), a primary GSK3 β substrate, was also decreased after SA-49 treatment (Fig. 6a, middle panel). To further investigate the effects of GSK3 β on SA-49-mediated MITF activity, we enforced expression of the wild type (WT), constitutively active (S9A) and kinase dead (K85A) GSK3 β in H460 cells and examined their impact on CLEAR luciferase activity. Both GSK3 β K85A mutant transfection and SA-49 treatment increased capacity to activate the CLEAR luciferase activity as compared with GSK3 β WT and S9A mutant (Fig. 6b), demonstrating GSK3 β inactivation promotes MITF transcription activity.

Next, we try to clarify the upstream kinase involved in SA-49-mediated GSK3 β inactivation. PI3K/Akt, protein kinase C α (PKC α), TGF- β -activated kinase 1 (TAK1) have been reported to regulate GSK3 β activity [37–39], we thus examined whether these kinases involved in SA-49-mediated GSK3 β inactivation by using the specific inhibitors. As shown in Fig. 6c, PI3K/Akt inhibitor LY294002 and TAK1 inhibitor 5Z-7-Oxozeanol failed to suppress SA-49-induced GSK3 β phosphorylation, however, PKC α / β inhibitor Go6976 dramatically abolished SA-49-induced GSK3 β phosphorylation. This data indicated that PKC α / β , but not PI3K/Akt or TAK1, involved in SA-49-induced GSK3 β inactivation. Indeed, SA-49 treatment induced a time- and dose-dependent PKC α / β phosphorylation in H460 cells (Fig. 6d). Furthermore, silence of PKC α , but not PKC β , abolished SA-49-induced GSK3 β phosphorylation and PD-L1 down-regulation (Fig. 6e and f). Altogether, these results suggest that SA-49 induces GSK3 β phosphorylation through a PKC α -mediated mechanism, thus promotes MITF nuclear translocation.

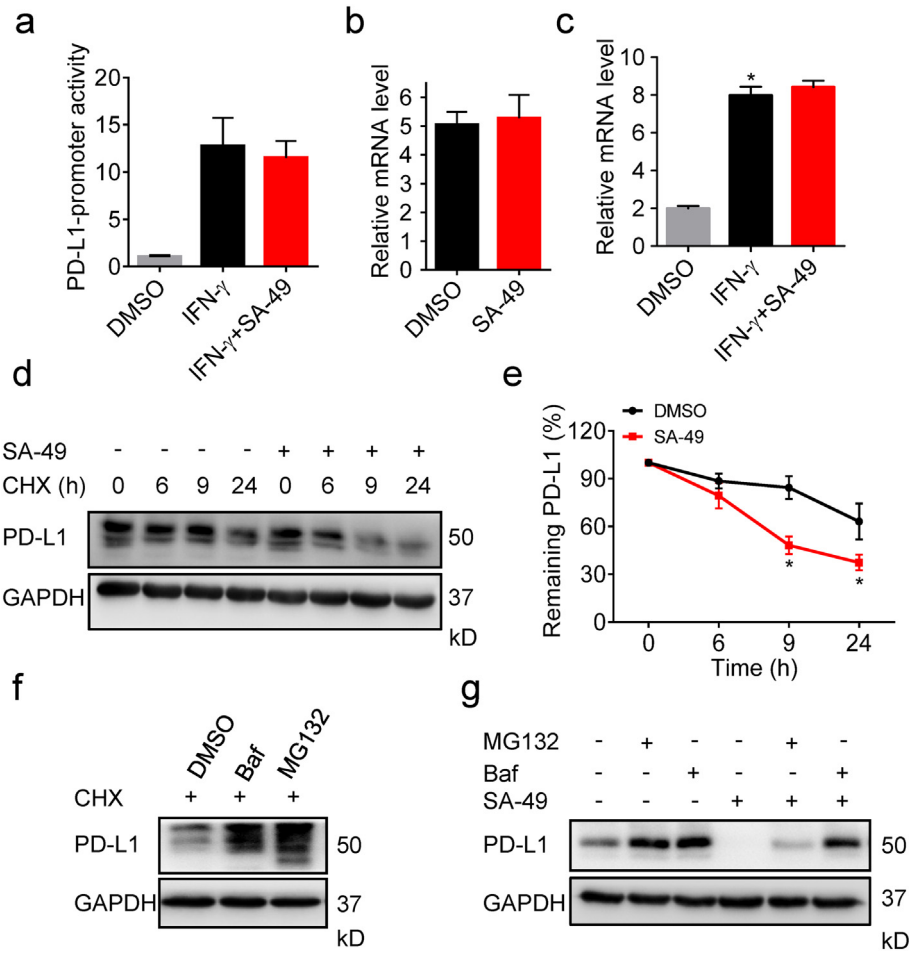


Fig. 3. Lysosomal pathway contributes to SA-49-mediated PD-L1 degradation. (a) The effect of SA-49 (10 μ M) on PD-L1 promoter activity in A549 cells stimulated with IFN- γ (5 ng/mL, 12 h) was determined by dual-luciferase assay. (b) Quantitative RT-PCR analysis of the mRNA level of PD-L1 in H460 cells treated with SA-49 (10 μ M, 12 h). (c) Quantitative RT-PCR analysis of the mRNA level of PD-L1 in A549 cells treated with SA-49 (10 μ M) and 5 ng/mL IFN- γ for 12 h. * p < 0.05 compared with DMSO group (n = 3, Student's t -test). (d) IB analysis of the PD-L1 expression in H460 cells treated with DMSO or SA-49 (10 μ M) for the indicated time points in the presence of CHX (25 μ g/mL). (e) Quantification of PD-L1 intensity in (d). The abundance was normalized to GAPDH; each group was normalized as a percentage of that at 0 h. * p < 0.05 compared with DMSO group (n = 3, Student's t -test). (f) Expression of PD-L1 determined by IB in H460 cells treated with Baf or MG132 in the presence of CHX (25 μ g/mL) for 24 h. (g) IB measuring the PD-L1 expression in H460 cells pre-treated with Baf or MG132, followed by SA-49 treatment for 24 h.

3.8. SA-49 suppressed tumor xenograft growth by activating immune microenvironment in mice

To determine whether SA-49 exert anti-NSCLC activity in vivo, we treated C57BL/6 mice bearing Lewis tumor xenografts with vehicle and SA-49 (20 mg/kg, 50 mg/kg, 100 mg/kg) via oral administration once a day for 20 days. As shown in Fig. 7a, the growth of Lewis tumor xenografts was inhibited dramatically following SA-49 treatment. The average tumor weight of the three SA-49-treated (20 mg/kg, 50 mg/kg, 100 mg/kg) groups were 0.73 ± 0.35 g, 0.96 ± 0.57 g and 0.61 ± 0.37 g respectively, which were significantly lower than that of the vehicle group (1.71 ± 0.89 g) (Fig. 7b). The tumor volume was also inhibited significantly following the injection of SA-49 (Fig. 7c). During the treatment period, SA-49 had no significant effect on the body weight of the mice (Supplementary Fig. 5a). Meanwhile, SA-49 did not remarkably alter the organ indexes including liver, spleen, heart, and kidney (Supplementary Fig. 5b), indicating that no systemic toxicity was observed after SA-49 treatment. To further evaluate the toxicity and side effects of SA-49, we collected the blood and organs at the last day, and conducted serum biochemistry analyses. The serum biochemical indices, including total protein (TP), blood urea nitrogen (BUN), creatine kinase (CK), alanine transaminase (ALT), aspartate aminotransferase (AST) showed no marked changes upon SA-49 treatment (Supplementary Fig. 6a). The H&E staining of kidney, spleen, liver and

heart also showed that SA-49 had no significant toxic effects on the major organs of mice (Supplementary Fig. 6b).

To investigate the role of SA-49 in antitumor immunity, we determined the expression level of related immunity molecules after SA-49 treatment in vivo. Immunohistochemistry assay indicated that the PD-L1 levels were decreased in Lewis tumor xenografts after SA-49 treatment (Fig. 7d and e, left panel). In addition, the number of CD3⁺ T cells were increased and FoxP3⁺ Treg cells were reduced (Fig. 7d and e, middle panel), indicating a shift toward an activated immune microenvironment rather than immunosuppressive [30]. Moreover, in tumor-infiltrating lymphocyte (TILs) profile analysis, the population of activated cytotoxic T cells (IFN- γ , CD3 and CD8 positive) in SA-49-treated tumors was significantly higher than that in control tumors (Supplementary Fig. 7), demonstrating that SA-49 could activate cytotoxic T cell in TILs. Because antitumor immunity is accompanied by apoptosis in tumor tissues, we compared the levels of cleaved caspase 3 and Ki67 (a marker of proliferation) and found that, cleaved caspase 3 was increased and Ki67 was decreased in SA-49-treated group (Fig. 7d and e, right panel). Notably, the phosphorylation levels of PKC α/β and GSK3 β were increased, while the expression level of PD-L1 was decreased in the tumors of SA-49-treated mice (Fig. 7f). These data suggested that SA-49 activates the immune microenvironment in tumor, which may contribute to its antitumor effects.

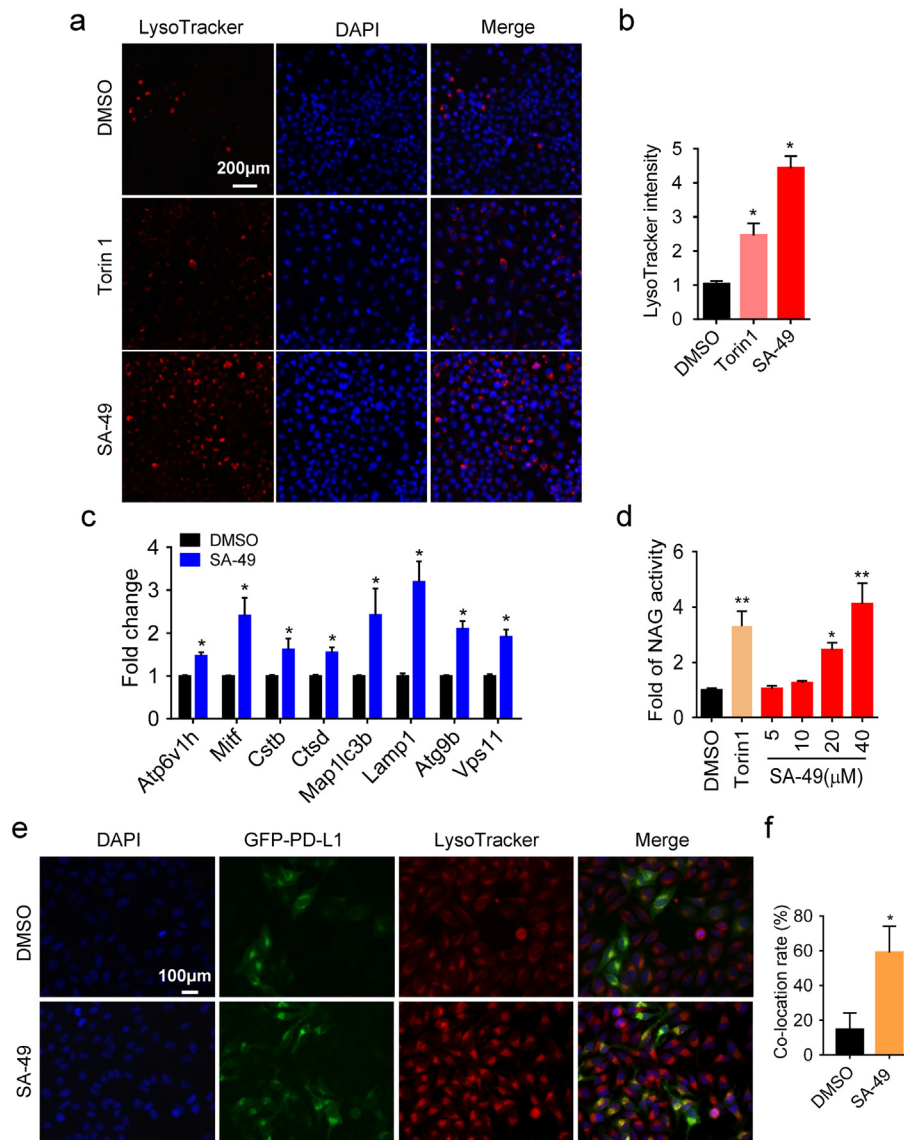


Fig. 4. SA-49 increases the biogenesis of lysosome and promotes translocation of PD-L1 to lysosome. (a) LysoTracker Red staining in H460 cells treated with SA-49 (10 μ M) or Torin1 (1 μ M) for 12 h. (Scale bar, 200 μ m). DAPI was used to label the nuclei. (b) Quantification of LysoTracker intensity of (a). * $p < 0.05$ compared with DMSO group ($n = 3$, Student's t -test). (c) H460 cells were treated with 10 μ M SA-49 for 12 h and subjected to qRT-PCR analysis. * $p < 0.05$ compared with DMSO group ($n = 3$, Student's t -test). (d) Relative lysosomal NAG activity of SA-49 and Torin1-treated H460 cells. * $p < 0.05$, ** $p < 0.01$ compared with DMSO group ($n = 3$, Student's t -test). (e) Fluorescent microscopy image showing the co-location of GFP-PD-L1 with LysoTracker in H460 cells treated with SA-49 (10 μ M) for 24 h. (Scale bar, 100 μ m). (f) Quantification of the merged intensity of (e). * $p < 0.05$ compared with DMSO group ($n = 3$, Student's t -test).

4. Discussion

Cancer cells exploit the expression of the PD-L1 to subvert T-cell-mediated immunosurveillance [40]. Small molecule inhibitors that disrupt PD-L1-mediated tumor tolerance are highly desirable. In the present study, we found SA-49, a new aloperine derivative with low cytotoxicity, as a potent antitumor agent via promoting the immunosuppressive co-signaling molecule PD-L1 degradation. PD-L1 was down-regulated by SA-49 in dose- and time-dependent manners in human lung cancer cells and in Lewis xenograft model. In addition, SA-49 increased the cytotoxicity of co-cultured T and NK cells, enhanced the number of CD3⁺ T cells and decreased number of FoxP3⁺ Treg cells in Lewis xenograft mice, thus activating the immune microenvironment in tumor. Furthermore, we demonstrated that the anti-tumor effect of SA-49 was through activating lysosome signaling induced by MITF translocation.

The role of lysosome in regulation of SA-49-mediated PD-L1 degradation is an important finding of this work. It has been reported

that PD-L1 is subjected to ubiquitin/proteasome-mediated protein degradation [29]. However, it is unlikely that SA-49 triggers PD-L1 degradation via the ubiquitin/proteasome mechanism for the following reasons. First, SA-49-induced PD-L1 reduction does not occur at the transcriptional level. Second, SA-49 did not mediate ubiquitination of PD-L1. Third, SA-49-induced proteolysis of PD-L1 was dramatically inhibited by the lysosomal inhibitor Baf but not the proteasome inhibitor MG132, suggesting that SA-49 promoted lysosomal proteolysis of PD-L1. Fourth, SA-49 triggered the translocation of PD-L1 to the lysosomes, indicating that PD-L1 could be degraded through the lysosomal pathway. Collectively, our findings reveal a novel mechanism by which SA-49 promotes lysosome-dependent degradation of PD-L1.

Lysosomes are cytoplasmic membrane-enclosed organelles containing hydrolytic enzymes that play a crucial role in degrading macromolecules and cell components [41,42]. Lysosome dysfunction causes cancer cell invasion and neurodegenerative disorders, while enhanced lysosome biogenesis promotes clearance of damaged

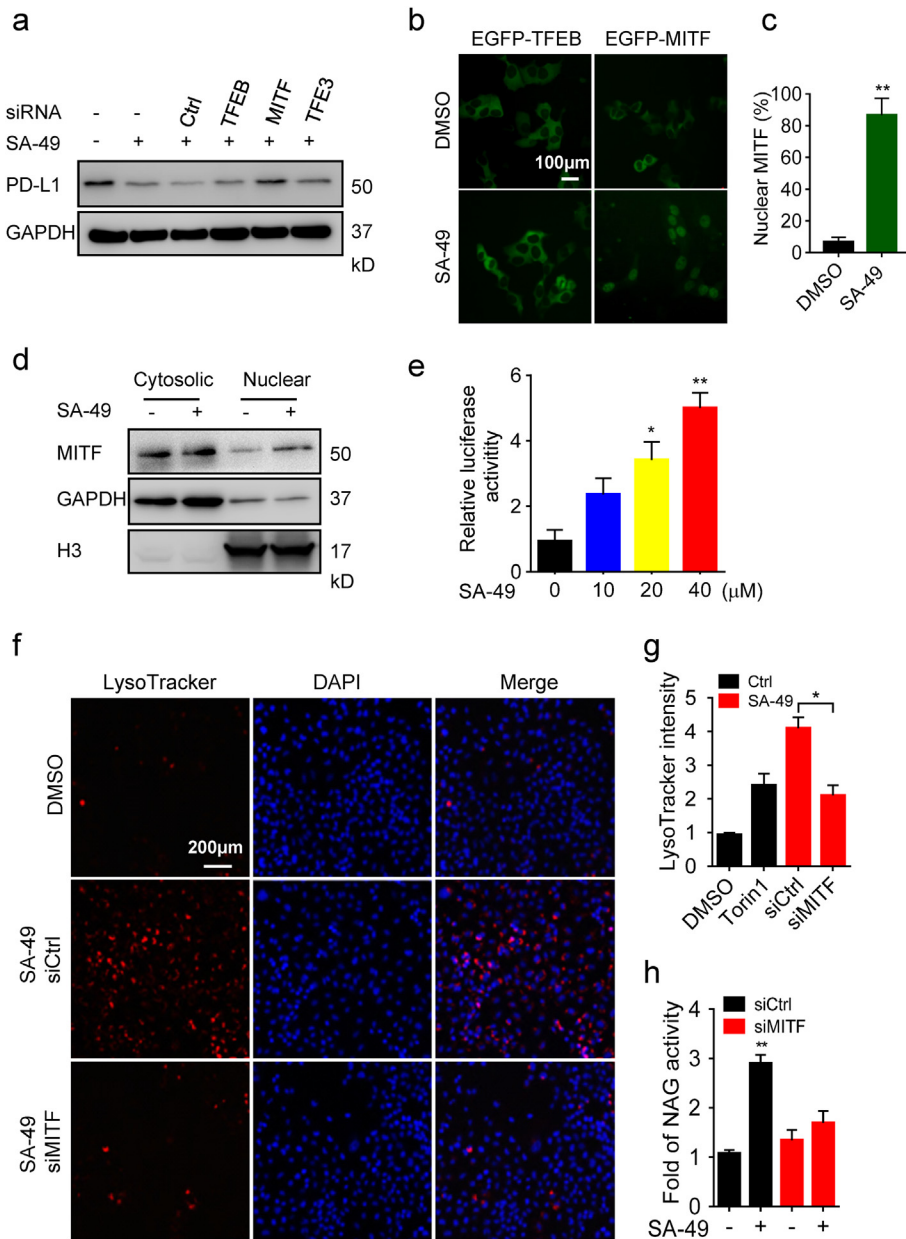


Fig. 5. SA-49 induces MITF-dependent PD-L1 degradation. (a) IB analysis of the PD-L1 expression in SA-49 (10 µM, 24 h)-treated H460 cells transfected with siRNAs-targeting control, TFEB, MITF or TFE3. (b) Fluorescent microscopy analyzing the subcellular distribution of TFEB and MITF in DMSO or SA-49 (10 µM, 12 h)-treated A549 cells. (Scale bar, 100 µm). (c) The percentage of cells with nuclear MITF was calculated, **p < 0.01 compared with DMSO group (n = 3, Student's t-test). (d) IB analyses of cytosolic and nuclear location of MITF in H460 cells treated with SA-49 (10 µM, 24 h). (e) Dual-luciferase assay verified the CLEAR activity in H460 cells treatment with the indicated concentrations of SA-49 for 6 h. *p < 0.05, **p < 0.01 compared with untreated control group (n = 3, Student's t-test). (f) LysoTracker Red staining in SA-49 (10 µM, 3 h)-treated H460 cells transfected with control or MITF siRNAs. (Scale bar, 200 µm). (g) Quantifications of LysoTracker Red intensity of (f). **p < 0.01 (n = 3, Student's t-test). (h) Relative lysosomal NAG activity after SA-49 treatment (10 µM, 24 h) in H460 cells transfected with control or MITF siRNAs. **p < 0.01 compared with untreated control group (n = 3, Student's t-test).

organelles or aggregated proteins [43,44]. Our LysoTracker staining results confirmed that SA-49 activate lysosome biogenesis in NSCLC cells, cell fractionation and confocal microscopy analysis indicated that PD-L1 was colocalized with LAMP1 (lysosome marker) and SA-49 promoted translocation of PD-L1 to the acid lysosomes for proteolysis, which is consistent with previous report that the YWHL-containing signal peptide in PD-L1 directed its localization in lysosomes [32]. How PD-L1 was degraded in lysosomes is by far less clear. Recent study demonstrated that CKLF-like MARVEL transmembrane domain containing protein 6 (CMTM6) co-localizes with PD-L1 at the plasma membrane and in recycling endosomes, where it prevents PD-L1 from being targeted for lysosome-mediated

degradation [45]. Whether CMTM6 is regulated by SA-49 and involved in lysosomal degradation of PD-L1 requires further investigations.

How lysosomal biogenesis occurs remains elusive. The microphthalmia family (MITF, TFEB, and TFE3) of transcription factors is known to be critical for regulation of lysosomal function and metabolism upon its translocation into the nucleus [46,47]. Our study demonstrated that SA-49 induced MITF, but not TFEB or TFE3-dependent lysosomal biogenesis in NSCLC. SA-49 treatment resulted in efficient MITF nuclear translocation and higher levels of lysosomal enzymes, thus enhancing lysosomal catabolic activity for PD-L1 degradation. In addition, MITF knockdown reversed SA-49-

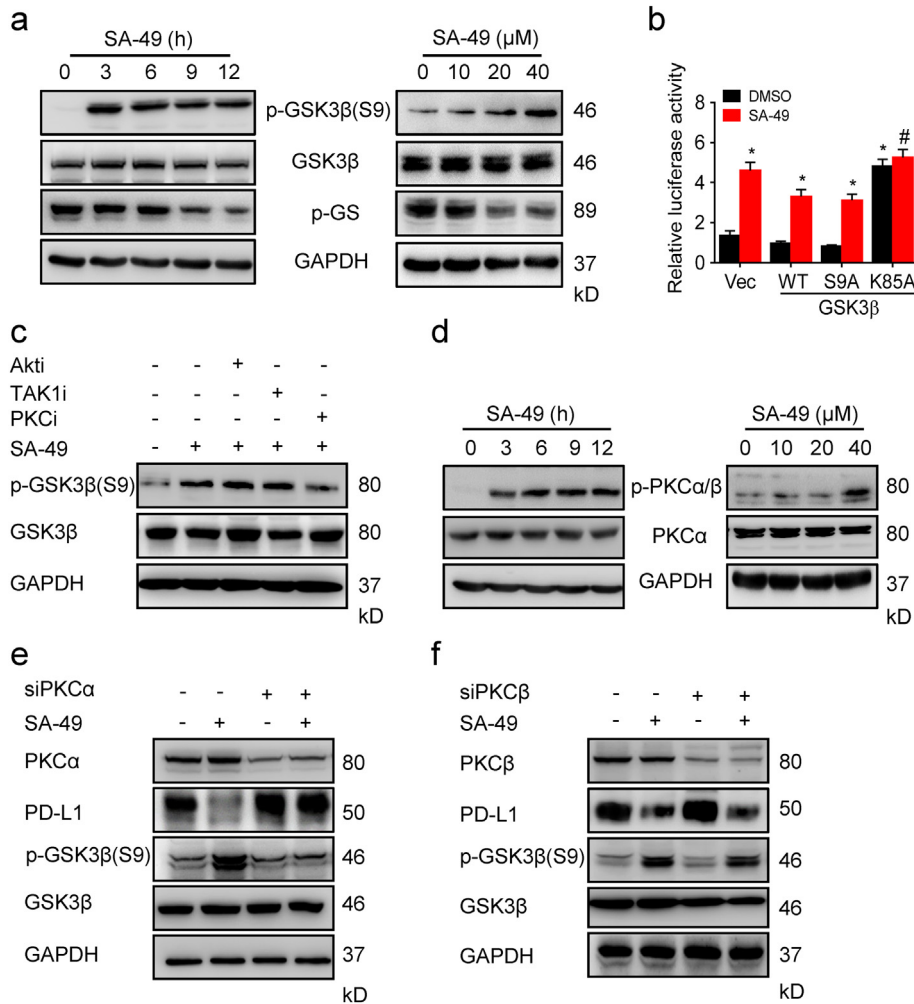


Fig. 6. PKC signaling is required for SA-49 action. (a) IB determined the levels of p-GSK3 β (S9), GSK3 β and p-GS in H460 cells treated with SA-49 (10 μ M) for the indicated time points (left panel), or the indicated concentrations for 24 h (right panel). (b) Dual-luciferase assay analyzed the CLEAR activity in H460 cells transfected with GSK3 β WT, S9A and K85A plasmids, followed by SA-49 (10 μ M) treatment for 12 h. * $p < 0.05$ ($n = 3$, Student's t-test) (c) IB analysis of the levels of p-GSK3 β (S9) and GSK3 β in H460 cells pretreated with LY294002 (Akti, 10 μ M), 5Z-7-Oxozaenol (TAK1i, 1 μ M), or Go6983 (PKC α / β i, 5 μ M) for 1 h, followed by SA-49 (10 μ M) treatment for 6 h. (d) IB analyzing the p-PKC α / β and PKC α levels in H460 cells treated with SA-49 (10 μ M) the indicated time points or the indicated concentrations for 24 h. (e and f) IB analysis of the PKC α , PKC β , PD-L1, p-GSK3 β (S9), and GSK3 β expression post-siRNA knockdown of PKC α or PKC β in SA-49 (10 μ M, 24 h)-treated H460 cells.

induced PD-L1 degradation in NSCLC. Our data thus linked MITF to PD-L1 regulation in cancer immunotherapy. Interestingly, SA-49 specifically activated MITF rather than TFEB or TFE3, suggesting that these three very similar transcription factors can be regulated by distinct mechanisms.

Our study provided evidences that SA-49 regulates lysosomal function and PD-L1 degradation via PKC α -dependent GSK3 β phosphorylation. Previous study showed that MTORC1 directly phosphorylates MiT/TFE proteins, resulting in retention of MITF in the cytoplasm. However, SA-49 had no effect on MTORC1 signaling, indicating that SA-49-induced MITF nuclear localization via an MTORC1-independent mode of action. On the other hand, our data demonstrated that SA-49 triggered GSK3 β inactivation and MITF transcription activity. Our results are in agreement with recent reports that GSK3 β inactivation promotes TFEB nuclear translocation [34]. To clarify the upstream signal involved in SA-49-induced GSK3 β inactivation, AKT, TAK1 and PKC activities were inhibited by specific inhibitors since these kinases have been reported to regulate the activation of GSK3 β . We found that inhibition of PKC activity by Go6976 or by PKC α siRNA abrogated SA-49-induced inactivation of GSK3 β . These observations suggest that PKC α , following activated by SA-49, inhibits GSK3 β activity and switches on MITF

nuclear translocation. How SA-49 activating PKC α needs further investigation.

Our study provides evidences that inactivation of GSK3 β indirectly modulation of PD-L1 stabilization via lysosomal dependent manner. In contrast, results from other analyses indicate that GSK3 β destabilized PD-L1 protein via phosphorylation. Li et al. revealed that glycosylation of PD-L1 prevents GSK3 β from binding to PD-L1, but GSK3 β phosphorylates the non-glycosylated PD-L1 4NQ and promotes its ubiquitination and fast protein degradation [2]. As PD-L1 is glycosylated in cancer cells, activation or inactivation of GSK3 β thus cannot directly interact with and regulate PD-L1 stabilization under normal physiological environment. Other mechanisms may involve in SA-49-induced, GSK3 β -mediated PD-L1 stabilization. Our finding of SA-49-induced lysosomal dependent PD-L1 degradation may provide another possibility of GSK3 β modulation of PD-L1 stabilization. In addition, GSK3 β binds to and phosphorylates PD-L1 protein in breast cancer cells, while our findings suggest that SA-49 induced MITF-dependent PD-L1 degradation in NSCLC cells. Thus, the role of GSK3 β in regulation of PD-L1 may depend on cell type or cell context. The comprehensive picture of GSK3 β regulation of PD-L1 needs further clarification.

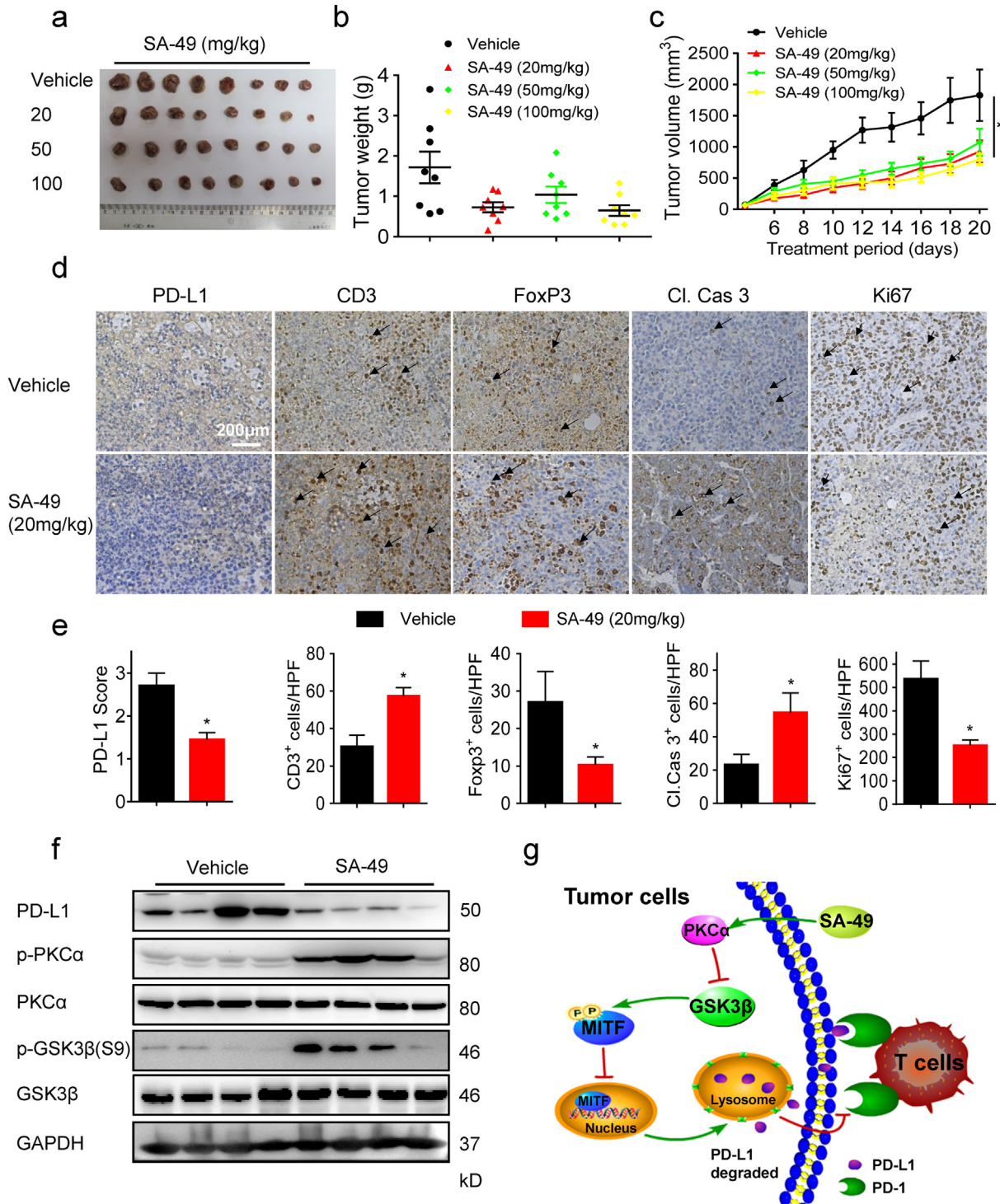


Fig. 7. SA-49 suppressed tumor xenograft growth by activating immune microenvironment in mice. (a) Images of tumor growth in mice treated with vehicle or SA-49 (20 mg/kg, 50 mg/kg and 100 mg/kg) were shown. (b and c) Quantification of tumor weight and tumor volume in vehicle or SA-49 treated-mice. (d) Representative immunohistochemical (IHC) staining results for PD-L1, CD3, FoxP3, cleaved caspase 3 and Ki67. (Scale bar, 200 μ m). (e) Quantification of IHC staining of (d). * $p < 0.05$ compared with vehicle group ($n = 3$, Student's t-test). (f) IB analysis of the levels of PD-L1, p-PKC α and p-GSK3 β in tumors separated from vehicle or SA-49-treated mice. (g) Proposed model of SA-49-mediated PD-L1 degradation by controlling PKC α -GSK3 β cascades to activate lysosomal function.

In summary, our study shows that SA-49 induces MITF-dependent lysosomal biogenesis and in turn degrades PD-L1 in NSCLC (Fig. 7g). SA-49 treatment activates PKC α and subsequently inactivates GSK3 β , which led to MITF nuclear translocation, boots the biogenesis of lysosome and promotes translocation of PD-L1 to lysosome for proteolysis. Therefore, our study reveals a novel mechanism by which SA-49

controls PKC α -GSK3 β cascades to activate lysosomal function and PD-L1 degradation. Our findings provide a rationale for the potential application of SA-49 as small molecule inhibitor that disrupts PD-L1-mediated tumor tolerance.

Supplementary data to this article can be found online at <https://doi.org/10.1016/j.ebiom.2019.01.054>.

Acknowledgements

We thank Dr. James Woodgett (University of Toronto, Canada) for kindly providing GSK3 β (WT, K85A, and S9A) plasmids.

Funding sources

This study was supported by grants from National Natural Science Foundation of China (81773782, 81473248 and 81621064), CAMS Innovation Fund for Medical Sciences (2016-12M-1-011) and Chinese Pharmaceutical Association-Yiling Pharmaceutical Innovation Fund for Biomedicine (GL-1-B04-20180366). The funding sources had no involvements in study design, data collection, data analysis, data interpretation, manuscript preparation and submission.

Author contributions

N. Zhang, Y. Dou and H. Deng designed this study; N. Zhang, Y. Dou, L. Liu, Y. Liu, and M. Ying performed the research and data analysis; X. Zhang, Q. Zeng and D. Song provided reagents, synthesized the aloperine derivatives and analyzed the data; X. Liu and Y. Dou performed the animal studies; H. Deng supervised the study and interpreted results; N. Zhang and H. Deng wrote and revised the manuscript.

Conflicts of interest

The authors have declared no conflicts of interest.

References

- Wei SC, Duffy CR, Allison JP. Fundamental mechanisms of immune checkpoint blockade therapy. *Cancer Discov* 2018;8(9):1069–86.
- Li CW, Lim SO, Xia W, Lee HH, Chan LC, Kuo CW, et al. Glycosylation and stabilization of programmed death ligand-1 suppresses T-cell activity. *Nat Commun* 2016;7:12632.
- Keir ME, Butte MJ, Freeman GJ, Sharpe AH. PD-1 and its ligands in tolerance and immunity. *Annu Rev Immunol* 2008;26:677–704.
- Boussiotis VA. Molecular and Biochemical Aspects of the PD-1 Checkpoint Pathway. *N Engl J Med* 2016;375(18):1767–78.
- Sharma P, Allison JP. Immune checkpoint targeting in cancer therapy: toward combination strategies with curative potential. *Cell* 2015;161(2):205–14.
- Sun C, Mezzadra R, Schumacher TN. Regulation and Function of the PD-L1 Checkpoint. *Immunity* 2018;48(3):434–52.
- Park SJ, Namkoong H, Doh J, Choi JC, Yang BG, Park Y, et al. Negative role of inducible PD-1 on survival of activated dendritic cells. *J Leukoc Biol* 2014;95(4):621–9.
- Sunshine J, Taube JM. PD-1/PD-L1 inhibitors. *Curr Opin Pharmacol* 2015;23:32–8.
- Bagley SJ, Bauml JM, Langer CJ. PD-1/PD-L1 immune checkpoint blockade in non-small cell lung cancer. *Clin Adv Hematol Oncol* 2015;13(10):676–83.
- Chen L, Han X. Anti-PD-1/PD-L1 therapy of human cancer: past, present, and future. *J Clin Invest* 2015;125(9):3384–91.
- Powles T, Eder JP, Fine GD, Braitht FS, Loriot Y, Cruz C, et al. MPDL3280A (anti-PD-L1) treatment leads to clinical activity in metastatic bladder cancer. *Nature* 2014;515(7528):558–62.
- Postow MA, Chesney J, Pavlick AC, Robert C, Grossmann K, McDermott D, et al. Nivolumab and ipilimumab versus ipilimumab in untreated melanoma. *N Engl J Med* 2015;372(21):2006–17.
- Petrella TM, Robert C, Richtig E, Miller Jr WH, Masucci GV, Walpole E, et al. Patient-reported outcomes in KEYNOTE-006, a randomised study of pembrolizumab versus ipilimumab in patients with advanced melanoma. *Eur J Cancer* 2017;86:115–24.
- Sheng J, Srivastava S, Sanghavi K, Lu Z, Schmidt BJ, Bello A, et al. Clinical pharmacology considerations for the development of immune checkpoint inhibitors. *J Clin Pharmacol* 2017;57(Suppl. 10):S26–42.
- Topalian SL, Taube JM, Anders RA, Pardoll DM. Mechanism-driven biomarkers to guide immune checkpoint blockade in cancer therapy. *Nat Rev Cancer* 2016;16(5):275–87.
- Dhanak D, Edwards JP, Nguyen A, Tummino PJ. Small-molecule targets in immunoncology. *Cell Chem Biol* 2017;24(9):1148–60.
- Cheng B, Yuan WE, Su J, Liu Y, Chen J. Recent advances in small molecule based cancer immunotherapy. *Eur J Med Chem* 2018;157:582–98.
- Wang H, Yang S, Zhou H, Sun M, Du L, Wei M, et al. Aloperine executes antitumor effects against multiple myeloma through dual apoptotic mechanisms. *J Hematol Oncol* 2015;8:26.
- Zhang L, Zheng Y, Deng H, Liang L, Peng J. Aloperine induces G2/M phase cell cycle arrest and apoptosis in HCT116 human colon cancer cells. *Int J Mol Med* 2014;33(6):1613–20.
- Chen S, Jin Z, Dai L, Wu H, Wang J, Wang L, et al. Aloperine induces apoptosis and inhibits invasion in MG-63 and U2OS human osteosarcoma cells. *Biomed Pharmacother* 2018;97:45–52.
- Zhang X, Liu Q, Zhang N, Li QQ, Liu ZD, Li YH, et al. Discovery and evolution of aloperine derivatives as novel anti-filovirus agents through targeting entry stage. *Eur J Med Chem* 2018;149:45–55.
- Wang YX, Pang WQ, Zeng QX, Deng ZS, Fan TY, Jiang JD, et al. Synthesis and biological evaluation of new berberine derivatives as cancer immunotherapy agents through targeting IDO1. *Eur J Med Chem* 2018;143:1858–68.
- Zhang N, Liu X, Liu L, Deng Z, Zeng Q, Pang W, et al. Glycogen synthase kinase-3 β inhibition promotes lysosome-dependent degradation of c-FLIPL in hepatocellular carcinoma. *Cell Death Dis* 2018;9(2):230.
- Liu L, Zhang N, Dou Y, Mao G, Bi C, Pang W, et al. Lysosomal dysfunction and autophagy blockade contribute to IMB-6G-induced apoptosis in pancreatic cancer cells. *Sci Rep* 2017;7:41862.
- Meier T, Uhlirk M, Chintharlapalli S, Dowless M, Van Horn R, Stewart J, et al. Tasisulam sodium, an antitumor agent that inhibits mitotic progression and induces vascular normalization. *Mol Cancer Ther* 2011;10(11):2168–78.
- Muhlbauer M, Fleck M, Schutz C, Weiss T, Froh M, Blank C, et al. PD-L1 is induced in hepatocytes by viral infection and by interferon-alpha and -gamma and mediates T cell apoptosis. *J Hepatol* 2006;45(4):520–8.
- Chen L. Co-inhibitory molecules of the B7-CD28 family in the control of T-cell immunity. *Nat Rev Immunol* 2004;4(5):336–47.
- Sandri M. Protein breakdown in cancer cachexia. *Semin Cell Dev Biol* 2016;54:11–9.
- Lim SO, Li CW, Xia W, Cha JH, Chan LC, Wu Y, et al. Deubiquitination and Stabilization of PD-L1 by CSN5. *Cancer Cell* 2016;30(6):925–39.
- Lastwika KJ, Wilson 3rd W, Li QK, Norris J, Xu H, Ghazarian SR, et al. Control of PD-L1 expression by oncogenic activation of the AKT-mTOR pathway in non-small cell lung cancer. *Cancer Res* 2016;76(2):227–38.
- Wang H, Yao H, Li C, Shi H, Lan J, Li Z, et al. HIP1R targets PD-L1 to lysosomal degradation to alter T cell-mediated cytotoxicity. *Nat Chem Biol* 2019;15(1):42–50.
- Durand-Panteix S, Farhat M, Youlyouze-Marfak I, Rouaud P, Ouk-Martin C, David A, et al. B7-H1, which represses EBV-immortalized B cell killing by autologous T and NK cells, is oppositely regulated by c-Myc and EBV latency III program at both mRNA and secretory lysosome levels. *J Immunol* 2012;189(1):181–90.
- Perera RM, Zoncu R. The lysosome as a regulatory hub. *Annu Rev Cell Dev Biol* 2016;32:223–53.
- Plopper D, Taelman VF, Robert L, Perez BS, Titz B, Chen HW, et al. MITF drives endolysosomal biogenesis and potentiates Wnt signaling in melanoma cells. *Proc Natl Acad Sci U S A* 2015;112(5):E420–9.
- Martina JA, Puertollano R. Rag GTPases mediate amino acid-dependent recruitment of TFEB and MITF to lysosomes. *J Cell Biol* 2013;200(4):475–91.
- Takeda K, Takemoto C, Kobayashi I, Watanabe A, Nobukuni Y, Fisher DE, et al. Ser298 of MITF, a mutation site in Waardenburg syndrome type 2, is a phosphorylation site with functional significance. *Hum Mol Genet* 2000;9(1):125–32.
- Hermida MA, Dinesh Kumar J, Leslie NR. GSK3 and its interactions with the PI3K/AKT/mTOR signalling network. *Adv Biol Regul* 2017;65:5–15.
- Li Y, Xu M, Ding X, Yan C, Song Z, Chen L, et al. Protein kinase C controls lysosome biogenesis independently of mTORC1. *Nat Cell Biol* 2016;18(10):1065–77.
- Bang D, Wilson W, Ryan M, Yeh JJ, Baldwin AS. GSK-3 α promotes oncogenic KRAS function in pancreatic cancer via TAK1-TAB stabilization and regulation of noncanonical NF- κ B. *Cancer Discov* 2013;3(6):690–703.
- Sharma P, Allison JP. The future of immune checkpoint therapy. *Science* 2015;348(6230):56–61.
- Efeyan A, Comb WC, Sabatini DM. Nutrient-sensing mechanisms and pathways. *Nature* 2015;517(7534):302–10.
- Settembre C, Fraldi A, Medina DL, Ballabio A. Signals from the lysosome: a control Centre for cellular clearance and energy metabolism. *Nat Rev Mol Cell Biol* 2013;14(5):283–96.
- Medina DL, Fraldi A, Bouche V, Annunziata F, Mansueto G, Spanpanato C, et al. Transcriptional activation of lysosomal exocytosis promotes cellular clearance. *Dev Cell* 2011;21(3):421–30.
- Xu H, Ren D. Lysosomal physiology. *Annu Rev Physiol* 2015;77:57–80.
- Burr ML, Sparbier CE, Chan YC, Williamson JC, Woods K, Beavis PA, et al. CMTM6 maintains the expression of PD-L1 and regulates anti-tumour immunity. *Nature* 2017;549(7670):101–5.
- Martina JA, Diab HI, Li H, Puertollano R. Novel roles for the MITF/TFE family of transcription factors in organelle biogenesis, nutrient sensing, and energy homeostasis. *Cell Mol Life Sci* 2014;71(13):2483–97.
- Slade L, Puliniikunil T. The MITF/TFE family of transcription factors: master regulators of organelle signaling, metabolism, and stress adaptation. *Mol Cancer Res* 2017;15(12):1637–43.